Chapter 2:
Review of Related Researches

2.1. Hyperspectral Remote Sensing

The phrase ‘remote sensing’ refers to the acquisition of information on the surface and the surrounding atmosphere of the earth and also those of the neighboring planets in the solar system through distant recording of the interaction of electromagnetic radiation of different wavelengths with the objects. This technique originated as a geographic tool where the mapping used to be done with aerial photography. Later it developed as a wide, interdisciplinary field of studies and applications in different disciplines of science and technology having the principles of physics in the background (Rees, 2001; Elachi, 2006; Scott, 2007). In a conventional remote sensing technique, the electromagnetic wave emitted, absorbed or diffracted by the object are recorded in several broad wavebands. The relative intensities of these bands are recorded in the images and the information on the targeted features are derived from images in terms of various ratios and algebraic combinations of reflectance values obtained at different wavebands (Jensen 2004). However, spectroscopic studies were no way related to the phenomena.

‘Spectroscopy’, as realized from literature (Bohr, 1922; Herzberg, 1944; Schawlow, 1982; Born and Wolf, 1999; Kleppner, 1999), is a technique for studying the structure of atoms and molecules by observing the interactions of only electromagnetic radiation of selective wavelengths with material objects. In addition to photons, subatomic particles like neutrons and electrons are also incorporated to the modern techniques of spectroscopy. The prime objective of spectroscopy is to study the radiation-material interaction or the interaction of subatomic particles and material atoms at different wavelengths of radiation and to achieve information on the atomic and molecular configuration of the material. The evolution of hyperspectral remote sensing has combined these two separate fields of earth science and physical science.

‘Hyperspectral’ or high spectral resolution in sensing provides a new dimension to the field of remote sensing (Vane et al., 1984; Goetz et al., 1985; Vane and Goetz, 1993; Green et al., 1998) that is an amalgamation of photography and spectrometry. The fundamental principle is to record images of the same object in narrow, contiguous wavebands over a large range of wavelengths. Then assembling all of the reflectance

values of the same pixel for each of the whole set of images, one can obtain a high-resolution spectrum, almost of laboratory quality, on the variation of reflectance with wavelength. Therefore, the technique is also known as *imaging spectroscopy*. The present work utilizes two types of hyperspectral images: airborne AVIRIS-NG and space-borne Hyperion introduced in Chapter 1. Their comparative features are now summarized in Table 2.1. Figure 2.1 presents a comparative view of imaging spectroscopy and field spectroscopy. The variation of radiance with wavelength is obtained for the radiation reflected from a typical vegetation both from the hyperspectral airborne image of AVIRIS-NG and the measured data of the ground-based spectroradiometer. Both are of almost the same quality.

Table 2. 1. Comparison of Hyperion and AVIRIS-NG

Features	**Hyperion**	**AVIRIS-NG**
Platform	Earth Observing-1 (EO-1) Sun-Synchronous Satellite	Airborne Flights
Spectral range	356 nm to 2577 nm	380 nm to 2510 nm
Spectral resolution	10 nm	5 nm
No. of channels	220 unique channels. VNIR (70 channels, 356 nm - 1058 nm), SWIR (172 channels, 852 nm - 2577 nm)	450 contiguous channels.
Ground swath	7.75 km	1.9 km to 11 km
Spatial resolution	30 m	≈ 4 m at 4 km flight altitude
Height	705 km	1.8 km to 5.3 km

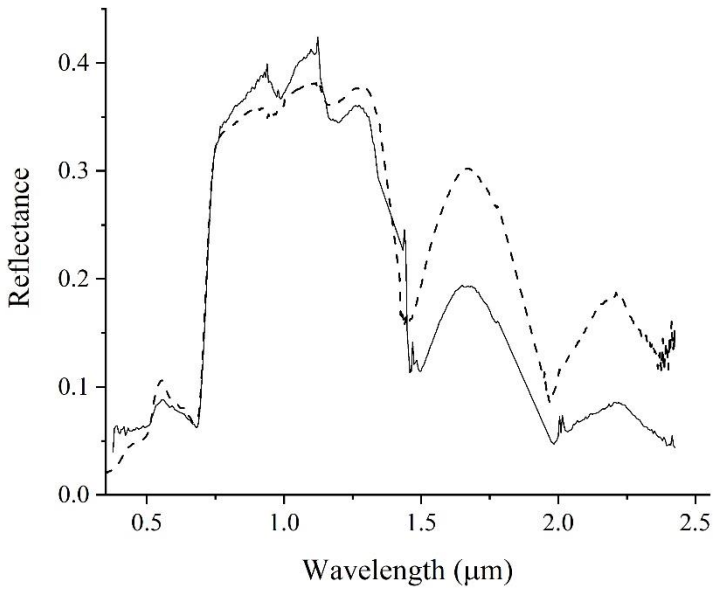

Figure 2. 1. Samples of radiance spectrum for the solar radiation reflected from a typical vegetation derived from AVIRIS-NG hyperspectral image (solid line) and measured with ground-based spectroradiometer (dashed line).

As reviewed in literature (Goetz, 2009; Raychaudhuri, 2016), the technique of hyperspectral remote sensing or imaging spectroscopy that provides with concurrent spatial and spectral data collection has been applied successfully to various fields of earth science, such as mineralogical mapping, studying vegetation species and physiology, properties of ocean, ice and snow, greenhouse gas monitoring and also to other disciplines, namely astronomy, medical science, and condensed matter physics. The present work has adopted hyperspectral imaging technique obtained with both airborne and satellite-borne sensors for assessing two important atmospheric parameters: carbon dioxide (CO_2) and aerosol. Ground-based spectral measurements carried out with spectroradiometer has been used as a reference for comparison.

2.2. Use of Spectroradiometer

A complementary and indispensable component of any remote sensing process is the procurement of ground truth. Corresponding to hyperspectral remote sensing, the ground truth is obtained with spectroradiometer.

A conventional spectrometer, generally used in undergraduate laboratories can determine the wavelength of a visible radiation accurately with human eye as sensor. Our human eye is an excellent hyperspectral sensor. However, it cannot measure the relative intensities at different wavelengths. Therefore, advanced laboratories use spectrophotometers that produce monochromatic light using grating, slit and white light. Photodetectors are used as sensors. The monochromatic light is made to be incident on material samples, such as semiconductor to understand its spectral behavior. The instrument needs dark room and is not portable. In the case of ground measurements for remote sensing, the instrument must be capable of acquiring spectra in bright daylight and should be portable. The spectroradiometer serves this purpose. The working principle of a spectroradiometer is outlined in Figure 2.2.

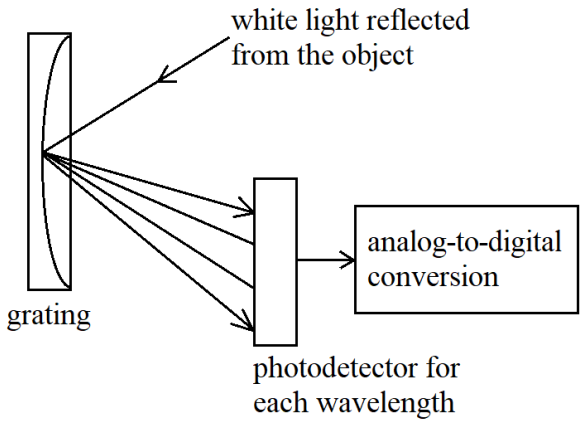

Figure 2. 2. Working principle of a spectroradiometer

A lens system collects the incident radiation (e.g., sunlight) that is either transmitted through the atmosphere or reflected from the object surface. The intensities of different wavelength components of the incoming radiation are modified according to absorption/scattering in the path and reflection/absorption at the object surface. Thus, the incident radiation carries all information on spectral signature. This is dispersed into

narrow wavebands by grating and an array of photodiodes detects the radiation intensities corresponding to each waveband.

The hyperspectral imaging sensor has a similar principle but each separated waveband is sent to a lens system to construct an image at that band. Each pixel of the image of each band records the digital number corresponding to the intensity in that band. Collecting all such data for all the images one can get the imaging spectrum for each pixel. Figure 2.3 compares such spectra obtained with ground-based spectroradiometer, airborne AVIRIS-NG and satellite-borne Hyperion. Figure 2.3(a) shows some samples of ground-based solar radiance spectra measured with spectroradiometer and Figure 2.3(b) presents some spectral samples derived from hyperspectral images. The present work has compared the CO_2 absorption bands obtained from all the three sources, as illustrated in Chapter 3.

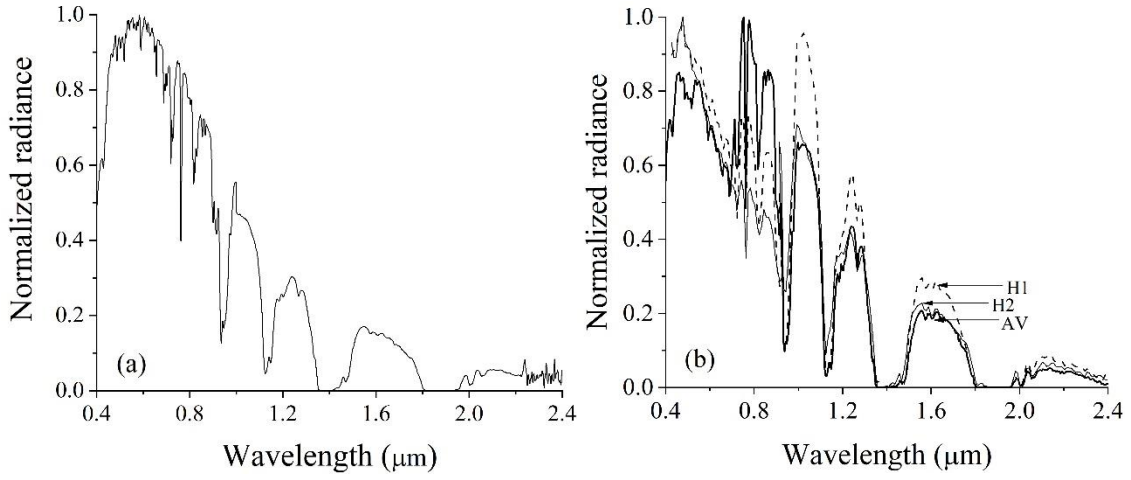

Figure 2. 3. Comparison of spectroradiometric and imaging spectra: (a) Samples of solar radiance spectra measured with ground-based spectroradiometer. (b) Samples of image-derived hyperspectral radiance variation for densely populated urban regions. The thick line marked as 'AV' denotes the radiance spectrum derived from AVIRIS-NG image and the thin lines represent the similar radiance spectra obtained from Hyperion images for monsoon (H1) and winter (H2) seasons.

2.3. Studies on Atmospheric Carbon Dioxide

The atmospheric carbon dioxide (CO_2), though exists in trace amount, exerts remarkable influences on global warming and irreversible climatic changes and has high vulnerability to human activities. Researchers have always been concerned with the existence of CO_2 as a greenhouse gas in the atmosphere and its ever-increasing concentration, particularly from the points of view of environment, ecosystem and future anticipation, as summarized in Table 2.2.

Table 2. 2. Several reports on the investigation of atmospheric CO_2 during the last six decades.

Reference	Major aspects of the study
Keeling, 1960	Variation of CO_2 concentration with season and latitude was estimated. The concentration was measured with gas analyzer.
Sawyer, 1972	Anticipated enhanced greenhouse effect of CO_2 produced by human activity.
Keeling, 1997	Effect of enhanced man-made CO_2 on climate change was apprehended.
Norby and Luo, 2004	Effect of rising CO_2 concentration on ecosystem was investigated involving multiple factors, such as vegetation, soil and environment.
Scheffer et al., 2006	The positive feedback, i.e. increasing effect of anthropogenic emissions on global temperatures was estimated based on reconstructed past changes.
Canadell et al., 2007	Rapid growth in fossil fuel CO_2 emissions and decline in the efficiency of CO_2 sinks on land and oceans were noted.
Solomon et al., 2009	Simulated that the climate change taking place due to increase in CO_2 concentration is largely irreversible. If all emissions were stopped, the removal of atmospheric CO_2 would be associated with slower loss of heat to the ocean and the atmospheric temperature would not drop significantly for at least 1000 years.
Zhong and Haigh, 2013	Simulated that the greenhouse trapping by CO_2 at different wavelengths is far from saturation and the greenhouse effect would increase at a faster rate, if the concentration exceeded 800ppmv.
Friend et al., 2014	Modeled that future climate change and rising atmospheric CO_2 levels are projected to have a significant impact on plant physiology throughout a vast section of the worldwide land area.
Ciais et al., 2019	Apprehension of uncertainty in the long-term trend of the northern land carbon sink.

It is noteworthy that majority of the above studies considered CO_2 around the surface level in either of the following three categories.

- Experimental determination of the gas concentration by chemical methods
- Use of previously reported results and
- Model generation based on simulated data.

The advent of hyperspectral remote sensing has added a new dimension to the CO_2 assessment that is the spectroscopic determination of the average concentration of the trace gas through the whole atmospheric column.

2.4. Hyperspectral Sensing of CO_2

The monitoring of atmospheric carbon dioxide (CO_2), an important greenhouse gas has got tremendous impetus during the last few decades. The physical principle of assessing the atmospheric CO_2 concentration is based on spectroscopic inversion of the extent of radiation absorption at specific wavelengths, proportional to the gas concentration, detected by ground based (Wunch et al., 2011; Andrews et al., 2014; Buschmann et al., 2016), airborne (Green 2001; Dennison et al., 2013; Thorpe et al., 2017) and space-borne (Bovensmann et al., 1999; Crisp et al., 2004; Hamazaki et al., 2004; Buchwitz et al., 2007; Kuze et al., 2009; Yokota et al., 2009; Bovensmann et al., 2010; Watanabe et al., 2015; Crisp et al., 2017) sensors.

The retrieval process involves a forward model for radiation as function of wavelength and gaseous concentration and a statistical inversion with reference to an initial prediction of the atmospheric state. Such techniques determine the average CO_2 concentration over the atmospheric column, which has a number of useful applications including estimating global CO_2 flux (Basu et al., 2013) and spatial distribution of anthropogenic sources (Hakkarainen et al., 2016; Janardanan et al.; 2016; Hakkarainen et al., 2019). The comparisons of such measurements are also studied (Buschmann et al., 2016; Wei et al., 2014; Wunch et al., 2017). Reports are available on global (Machida et al., 2008; Yoshida et al., 2011; Crisp et al. 2017), regional (Tiwari et al., 2013, 2014; Ravi Kumar et al. 2014, 2016; Hakkarainen et al., 2016; Umezawa et al., 2018; Gupta et al.

2019) and local (Huang et al., 2015; Xueref-Remy et al., 2018; Imasu and Tanabe, 2018; Roman-Cascon et al., 2019) CO_2 assessments.

The present work has utilized the satellite-borne data of mainly Orbiting Carbon Observatory-2 (OCO-2) data. Also Atmospheric Infrared Sounder (AIRS) data are used sometimes for comparison. It is relevant to mention that OCO-2 detects CO_2 at two absorption bands centred about 1.61 μm and 2.06 μm, referred to as 'weak absorption' and 'strong absorption', respectively (Crisp et al., 2017) whereas AIRS retrieves CO_2 utilizing 15 μm band of the spectrum (Wei et al., 2014).

High spatial resolution mapping of carbon dioxide (CO_2) concentration levels from atmosphere has gained importance as a supplement to global CO_2 monitoring with ground-based and satellite-borne sensors in connection with validating satellite measurements and detecting localized variations in CO_2 concentrations caused by natural disturbances such as volcanic eruption and anthropogenic sources such as power plants. The first airborne imaging sensor to detect the reflected solar radiation spectrum at high spectral and spatial resolution, the Airborne Visible Infrared Imaging Spectrometer (AVIRIS), has been successfully applied to analyze atmospheric trace gases and water vapour. The sensors in this category do not have the same spectral resolution as the specialized sensors for greenhouse gases and are unable to follow the actual physical process of radiation absorption, which is a sub-nanometer phenomenon. These can only detect an average absorption spectrum spanning several nanometers. These, on the other hand, offer higher spatial resolution and the capacity to record local alterations in terrestrial properties. A sensor with a very high accuracy of spectral resolution may have a poorer spatial resolution. As a result, nanometer-level imaging sensors with improved spatial resolution may identify trace gas point sources, precisely monitor local atmospheric changes, and provide helpful methods for future space-borne imaging. The significance of such narrowband channels for gaseous absorptions and point sources of the gaseous emission is recognized in Chapter 4.

2.5. Seasonal Variability of CO_2

The overall trend of the seasonal variations of atmospheric CO_2 concentrations shows a constant increase with time, which is overlaid by an oscillating seasonal oscillation (Keeling et al., 1976; Keeling et al., 2005; Basu et al. 2014; Imasu and Tanabe, 2018). In general, the amplitude of the yearly change is greater in the northern hemisphere than in the southern hemisphere (Dettinger and Ghil, 1998; Keeling et al., 2005; Jiang et al., 2016). Seasonal fluctuation in atmospheric CO_2 content has been a well-documented occurrence for over half a century. The seasonal development of terrestrial plants, which causes CO_2 intake and release, has been identified as the cause of such periodic shift (Keeling et al., 1996; Buermann et al., 2007; Basu et al. 2014).

However, additional intriguing aspects of CO_2 concentration are testified to all the way through, preserving the topic's attractiveness. Several examples include the occurrence of the maximum and minimum CO_2 concentrations in two different seasons for the northern and southern hemispheres (Monfray et al., 1987; Nevison et al., 2008), semiannual fluctuation (Jiang et al., 2016) and simulated effect of fossil fuel emission on the sub-annual variation of CO_2 concentration (Zhang et al., 2016), and the effects of Madden-Julian Oscillation (Li et al., 2010) and El Nino events (Keeling et al., 1996; Nevison et al. 2008; Jiang et al., 2013) on CO_2 concentration. The greenhouse contribution of CO_2 and related global climate changes (Kondratyev and Varotsos, 1995), long-term persistence in CO_2 concentration variation (Varotsos et al., 2007), and atmosphere-ocean CO_2 exchange (Krapivin and Varotsos, 2016) are all being investigated. There have been studies on the relationship between CO_2 and climate variability, including rainfall (Tiwari et al., 2013) and sea surface temperature (Ravi Kumar et al., 2016), regional variability (Tiwari et al., 2014), interannual variability of tropical carbon balance in connection to climate-driven fluctuations (Fu et al., 2017), and the influence of non-uniform global warming on the seasonal cycle of CO_2 variation (Li et al., 2018).

Recent research on CO_2 seasonal fluctuations encompasses a variety of factors, including the association of climatic effect with gross primary production (GPP) (Lee et al., 2018), biosphere and anthropogenic seasonal CO_2 contributions (Xueref-Remy et al.,

2018), seasonal variability of CO_2 partial pressure in water bodies (Marescaux et al., 2018), and the influence of wind direction (Roman-Cascon et al., 2019) on CO_2 mixing ratio. Concerns regarding the lack of agreement on the key mechanisms raising CO_2 seasonal amplitude (Piao et al., 2018) and attempts to forecast its future trajectory (Zhao and Zeng, 2014) highlight the topic's relevance. The present studies on the seasonal changes of CO_2 and related explanations are elaborated in Chapter 6.

2.6. CO_2 in India

As outlined above, the technique of hyperspectral remote sensing, sometimes referred to as imaging spectroscopy is widely applied to the field of global monitoring of atmospheric CO_2 with satellite-borne, airborne and ground-based sensing systems. Yet the CO_2 sensing in Indian context has some distinguished features, as follows.

(A) Vastness: India is a huge (≈ 3287263 km2, 6.7–35.5º N, 68.11–97.42º E) and highly populated (≈ 1210 million as on March 2011) country with differentiated geographical features. A large portion of the installed generation capacity (≈ 65 % of 344002 MW) is dependent on fossil fuels (Govt. of India, 2019; India, 2020; Roy et al., 2015). The energy consumption in India has almost tripled during 1991-2013 and the CO_2 emission, with certain specifications, has got enhanced from 779 to 1574 million tons during 1994–2010 (Garg et al., 2017). These facts highlight the significance of exploring the past and present trends of CO_2 over the Indian atmosphere.

(B) Long Legacy: Indeed diversified aspects of CO_2 in the Indian context have already been studied so far that include the simulation of climatic variability with CO_2 enhancement (Bhaskaran et al., 1995), energy consumption and CO_2 emission (Majumdar and Gajghate, 2011), CO_2 and energy flux at forested (Jha et al., 2013) and rural (Patil et al., 2014) zones, connotations with rainfall (Tiwari et al., 2013; Singh et al., 2015) and circulation of monsoon (Revadekar et al., 2016), sequestration potential (Garg et al., 2017a), temporal change (Chhabra and Gohel,

2017) and comparison of the recent CO_2 column averages of several Indian sites with that of other places at global level (Raychaudhuri and Roy, 2022).

(C) Unexplored Facets: In spite of the above-mentioned studies, some significant factors have remained uncultivated and some new features are expected with the CO_2 of India. A few are highlighted below.

- In the tropical atmosphere of India, the atmospheric water vapour (H_2O) is a major entity and the high quantity of H_2O is likely to cast significant influence on the CO_2 absorption band and the resultant CO_2 retrieval.
- The extensive vegetated regions of India and the surrounding seas are likely to be in support of CO_2 sequestration and the balance of emission and confiscation in this connection should be investigated.
- Also, it is necessary to correlate the present tendency of atmospheric CO_2 in India with the previously reported results.
- Hyperspectral remote sensing techniques have seldom been applied to the CO_2 assessment in India.

Considering the above scopes for exploring the CO_2 trends in India and availing the opportunity of the AVIRIS-NG hyperspectral imaging for the first time in India (Chapter 3), the present work has assessed the spatial and temporal changes (Chapter 4) and the seasonal variations (Chapter 6) of CO_2 over the Indian atmosphere.

2.7. Recent CO_2 Scenario at Global Level

Although the primary goal of this study was to investigate the suitability of OCO-3 in estimating the yearly change in xCO_2, coincidently this new sensor has been subjected to the worldwide restricted fossil fuel burning situation caused by the novel coronavirus (COVID-19). A recent set of papers (Table 2.3) investigated the influence of the COVID-19 pandemic-related worldwide lockdown on atmospheric CO_2. An overall conclusion was that the surface-level CO_2 emissions were reduced to a substantial amount, but the

effect on the column average was negligible. Furthermore, there was a high degree of unpredictability in the data, as well as inaccuracies in the sequence of observation. Nonetheless, the current study addresses just a few issues for additional investigation.

Many of the studies are regional in nature and do not account for the full-year CO_2 change in 2020. The column mixing of CO_2 with air is a lengthy process, and surface changes are unlikely to be reflected promptly in the column average. Also, there is a considerable variance in CO_2 drop from place to location, as discovered in the current study. Table 2.3 provides a basic comparison.

Table 2. 3. Overview of several studies on the sudden decrease of CO_2 emissions and the resulting changes in column averaged dry-air mole fractions of CO_2 (xCO_2) during the worldwide lockdown caused by the COVID-19 outbreak.

Reference	Data source	Study Region	Findings	Constraints and Conclusions
Sussmann et al., 2020	TCCON sites	Mid-latitude, 46–49°N, 90°W–11°E	Projected annual CO_2 emission reduction for 2020 up to ≈ 8%.	Forecast uncertainty, improved terrestrial ecosystem models are required for better quantifying land and ocean sinks.
Tohjima et al.,2020	Hateruma Island Station, Japan	Chinese provinces	Estimated fossil fuel CO_2 reduction 32 ± 12% in Feb.2020 and 19 ± 15% in Mar.2020.	10% reduction of the global emissions corresponds to only ~ 0.5 ppm reduction in xCO_2, a maximum of 0.8 ppm over China whereas per year increases is ~ 2 ppm with large variability
Chevallier et al., 2020	OCO-2	Global model simulation	0.5 to 2 ppm decrease in regional xCO_2 at various places	The impact of the emission reduction is mainly local; may be isolated but cannot be quantified accurately. The cloud condition is also an issue.
Le Quéré et al., 2020	government policies and activity data	Global: US, China, Europe, India	Reduction of 11 to 25% in daily fossil CO_2 emissions during the forced confinement.	Present satellite measurements are not suitable for near-real time determination of anthropogenic contribution to CO_2 column average because of large uncertainties and the variability of the natural CO_2 fluxes
Liu et al., 2020	Near-real-time activity data from Carbon Monitor research initiative and xCO_2 from GOSAT	Global: US, China, Europe, India, Brazil	Abrupt 8.8% decrease in global CO_2 emissions in the first half of 2020	Satellite and ground observed nitrogen dioxide (NO_2) column concentration exhibited a decrease consistent with the reduction of fossil carbon fuels emissions.

Buchwitz et al., 2021	OCO-2 and GOSAT	East China, 28–44°N, 102–126°E	Emission reduction by approximately 10% ± 10%. The expected xCO_2 reduction is only ~ 0.1 – 0.2 ppm.	Sparseness of the satellite data, month-to-month variability. Consistent detection and accurate quantification of the emission reduction with the current satellite data sets is challenging.
Zeng et al., 2020	GOSAT and ODIAC emissions database	Global: East Asia, China, Europe, US and India	Lockdown-related drop of 10-20 ppm at discrete cities	7.9% reduction in emissions for 4 months would result in 0.25 ppm decrease in the Northern Hemisphere CO_2, a few times smaller than natural variabilities. Need of improved accuracy and expanded spatiotemporal coverage of monitoring systems was realized.
Weir et al. 2020	OCO-2	Global: US, Europe, Aisa	The regional impact of COVID-19 was observable from space. The monthly CO_2 emissions from fossil fuel use decreased up to 20% for a given day and 4-7% by April, 2020.	xCO_2 over largest emitting regions was 0.24 to 0.48 ppm less, consistent with 5–10% reduction in annual global fossil fuel emissions. Just above OCO-2 detection limit, still distinguishable from climate-driven anomalies. Improvement and collaboration of monitoring systems with greater emphasis on fossil fuel emissions is suggested.
The present work	OCO-3	Globally distributed 2°×2° locations, nine urban (20 to 50° N), nine unpopulated (50° N to 30° S)	Clear indication of reduction in CO_2 column average, at urban regions, during the COVID-19 pandemic, 2020.	Wavelet coherence technique is suggested for quantifying that temporary reduction using the OCO-2 data as reference.

Abbreviations:

TCCON: Total Carbon Column Observing Network (ground-based)

GOSAT: Greenhouse Gases Observing Satellite

OCO-2 and OCO-3: mentioned in the main text

ODIAC: Open-source Data Inventory for Anthropogenic Carbon dioxide

2.8. Relevant Parameters

2.8.1. Solar-Induced Chlorophyll Fluorescence

Under the stimulation of the shorter wavelength (e.g., blue) fraction of solar radiation, the chlorophyll molecules of healthy green vegetation produce a modest emission in red and near-infrared wavelengths. This solar-induced chlorophyll fluorescence (SIF) is a crucial physiological feature of vegetation that is directly connected to carbon absorption via photosynthesis resulting the oxygen–carbon dioxide equilibrium in the atmosphere.

The principle of retrieving SIF from space is based on the in-filling of solar Fraunhofer line depths in the presence of SIF emission from the earth's surface. The primary goal of OCO-2 (and also OCO-3) is to estimate the CO_2 column averaged dry air mole fraction (xCO_2) from space, but SIF can also be retrieved concurrently using spectral measurements in the oxygen absorption band (0.757–0.775 μm) that overlaps with the SIF emission spectrum (0.660–0.850 μm). The SIF ($Wm^{-2}sr^{-1}\mu m^{-1}$) is calculated by filling solar Fraunhofer lines in small spectral windows about 0.757 μm and 0.771 μm. The details of estimating the column-averaged concentration of atmospheric CO_2 and SIF from the spectroscopy of the reflected solar radiation are available in literature (Frankenberg *et al*. 2012, Sun *et al*. 2018). It may be mentioned that the CO_2 exchange with vegetation during photosynthesis, quantified as GPP is positively related with SIF (Joiner et al., 2014; Miao et al., 2018). The use of SIF data in support of CO_2 assessment are elucidated in chapters 6 and 7.

2.8.2. Atmospheric Aerosols

Aerosols are suspended particles in the atmosphere having either natural origin, such as marine salt, volcanic ash and biological debris or man-made sources, such as black carbon and industrial dust. Aerosols can influence the global climate significantly through absorption and scattering of radiation solar radiation and take important part in cloud formation, precipitation, pollutant transport, and other atmospheric phenomena.

Aerosol impacts are assessed using both active lidar remote sensing (David et al., 2012) and passive radiometric (Kaufman et al., 1997) observations. International partnerships on ground-based aerosol measurements, such as AERONET (Holben et al., 1998) and EARLINET (Matthais et al., 2004) are established. Aerosol estimate is carried out using several satellite-based systems such as MODIS (Remer et al., 2005), METEOSAT (Elias and Roujean, 2008), POLDER & MERIS (Dubuisson et al., 2009) and SCIAMACHY (Sanghavi et al., 2012). For all such studies, the *optical depth* or *optical thickness* of the aerosol is an essential metric in the assessment of the spatial distribution, particle concentration, and size. It is assessed by applying the Beer-Bouguer-Lambert law and knowing the amount of radiation transmitted through the atmosphere at certain wavelengths. Table 2.4 presents a brief account of the physical principles generally used for the retrieval of aerosol optical depth.

Generally the radiation values at the wavelengths of less attenuation are preferred for the calculation of aerosol optical depth and the extra-terrestrial radiation near the top of the atmosphere is required as a reference. The present work has addressed the aerosol optical depth from a different angle of atmospheric oxygen absorption band. The related mathematical model and validation with satellite images are depicted in Chapter 5.

Table 2. 4. A brief sketch of several well-known methods of assessing aerosol optical depth.

Source of measurement	Physical principles involved	References
Moderate Resolution Imaging Spectroradiometer (MODIS) aboard both NASA's *Terra* and *Aqua* satellites	Visible blue (0.47 μm), red (0.66 μm) and shortwave infrared (SWIR) (2.13 μm or 2.2 μm) wavelengths are involved in the aerosol estimation. The key factor is the difference in surface reflectance for these wavelengths. The SWIR (≈ 2 μm) wavelength is much larger than the size of most of the aerosols and the aerosols appear to be transparent to solar radiation so that the surface reflectance is quite different from the other two. The extent of reflectance also distinguishes "land" pixels or "water" pixels. The existence of subpixel water is screened by detecting small (< 0.1) values of the Normalized Difference Vegetation Index for each pixel.	Kaufman et al., 1997 Remer et al. 2005

Polarization and Directionality of Earth's Reflectances (POLDER) aboard ADEOS-1 satellite	Directional polarization measurements detect the polarized light that the aerosols backscatter and the top-of-atmosphere measurements of the polarized light reflected by the earth surface is more tractable than the total reflected light.	Deuze et al. 2001
Ground-based sun-sky scanning radiometer system	Solar photometry is carried out at different visible and near-infrared wavelengths and the spectral sky radiance is measured at known angular distances from the Sun. spectral extinction of direct beam radiation according to the Beer-Lambert-Bouguer law. A number of such systems are networked at regional to global scale.	Holben et al., 1998

2.8.3. Wavelet Analysis

Traditional mathematical approaches for investigating the periodicity of a time series in frequency domain, such as Fourier analysis, presume that the temporal variation is stationary. However, wavelet analysis has proven to be a useful tool in the case of multidimensional time series, such as non-stationary signals, localised fluctuations, or intermittent periodicities. It has been used to understand geophysical and atmospheric phenomena on several occasions.

The initial stage in wavelet analysis is to define a wavelet that will be compared to the signal or time series under consideration. A wavelet is a wave-like functional form that is not continuous but increases and decreases over a brief period of time. The integral of the wavelet function $\psi(t)$ over time (t) is zero, implying that

$$\int_{-\infty}^{\infty} \psi(t)dt = 0 \tag{2.1}$$

The wavelet has a rapid amplitude decay in time, implying that

$$\int_{-\infty}^{\infty} |\psi(t)|^2 dt = 1 \tag{2.2}$$

As a result, the wavelet is a zero-mean function that is confined in both frequency and time. Wavelet has various standard functional shapes. The present study adopts the Morlet wavelet, which is complex exponential modulated by Gaussian given by

$$\psi(t/s) = \pi^{-1/4} e^{i\omega(t/s)} e^{-\frac{1}{2}(t/s)^2} \tag{2.3}$$

In Eq. (2.3), t symbolizes time, s denotes the wavelet period, also known as scale, which renders time dimensionless, and ω refers a non-dimensional frequency. For instance, if ω = 6, the Gaussian envelope contains about three oscillations.

The wavelet transform of a time series x_n, n = 1,…, N with uniform time interval δt and the specified wavelet function ψ may be represented schematically as

$$W(s) = \sqrt{\frac{\delta t}{s}} \sum_{m=1}^{N} x_m \psi\left[(m-n)\frac{\delta t}{s}\right] \tag{2.4}$$

The wavelet filters the time series like a band pass filter and is stretched in time (t) by adjusting its size (s). The wavelet transform can be continuous (ideal for feature extraction) or discrete (not good for feature extraction) (useful to noise reduction and data compression). The continuous wavelet transform is used in this study.

$$W_{x,y}^{a,b} = \frac{\left|S(W_x^*(a,b)W_y(a,b))\right|^2}{S(\left|W_x(a,b)\right|^2).S(\left|W_y(a,b)\right|^2)} \tag{2.5}$$

Eq. (2.5) represents the wavelet coherence between two time series x and y, which is a measure of their correlation. The continuous wavelet transformations of x and y at scale a and position b are denoted by $W_x(a,b)$ and $W_y(a,b)$, respectively. The complex conjugate is represented by the superscript (*), and S is a smoothing operator that performs a weighted running average in both time and scale.

A phase arrow in the wavelet cross spectrum represents the phase difference between the two time-series visually. A right arrow indicates that x and y are in phase, a left arrow indicates that they are anti-phase, an upward arrow indicates that y leads x by 90°, and a downward arrow indicates that x leads y by 90°. The phase angle may be computed from the phase arrows, and the distribution of phase angles in the highly coherent zone offers a quantitative notion of how far apart the two signals are. Interquartile Range (IQR) appears to be the best technique for estimating the spread of phase angles for an unknown distribution. The difference between the upper and lower quartiles, Q_3 and Q_1, of a set of data is used to determine the IQR. The first quartile (Q_1)

is the median of the n smallest values, and the third quartile (Q_3) is the median of the n biggest values, given an even ($2n$) or odd ($2n+1$) number of values. The second quartile (Q_2) corresponds to the ordinary median. The overall phase difference of x and y is determined by the IQR of phase angles.

The present work has utilized the wavelet analysis technique for analyzing the seasonal CO_2 fluctuation using OCO-3 data (Chapter 7) in a two-step process. To develop a reference for OCO-3 to compare against while maintaining both spatial and temporal consistency. The former is obtained using fitted annual variations derived from the database of its forerunner OCO-2 for a specific region, whereas the latter is obtained using the time-frequency decomposition of wavelet analysis technique applied to the time-variation of the spatial parameter (xCO_2) using Morlet waveform (plane wave modulated by Gaussian function) as the parent wavelet. The 3rd order polynomial fitted curves for the xCO_2 yearly fluctuation of each region acquired from both OCO-3 and OCO-2 were used to create the fundamental building blocks for the continuous wavelet transform. To determine the presence of any probable localized consistency in phase, wavelet coherence analysis was performed for two sets of time series: OCO-2,'18, OCO-2,'19 & OCO-3,'20 and OCO-2,'18, OCO-2,'19 & OCO-2,'20 for each of the urban zones.

Chapter References

Andrews, A. E., Kofler, J. D., Trudeau, M. E., Williams, J. C., Neff, D. H. & Masarie, K. A. et al. (2014). CO_2, CO, and CH_4 measurements from tall towers in the NOAA Earth System Research Laboratory's Global Greenhouse Gas Reference Network: instrumentation, uncertainty analysis, and recommendations for future high-accuracy greenhouse gas monitoring efforts. *Atmospheric Measurement Techniques*, 7(2), 647-687. doi: 10.5194/amt-7-647-2014

Basu, S., Krol, M., Butz, A., Clerbaux, C., Sawa, Y. & Machida, T. et al. (2014). The seasonal variation of the CO2 flux over Tropical Asia estimated from GOSAT, CONTRAIL, and IASI. *Geophysical Research Letters*, 41(5), 1809-1815. doi: 10.1002/2013gl059105

Bhaskaran, B., Mitchell, J., Lavery, J., & Lal, M. (1995). Climatic response of the Indian subcontinent to doubled CO_2 concentrations. *International Journal Of Climatology*, *15*(8), 873-892. doi: 10.1002/joc.3370150804

Bohr, N. (1922). *The theory of spectra and atomic constitution*. Great Britain: Cambridge University Press.

Born, M., & Wolf, E. (1999). *Principles of Optics* (7th ed.). UK: Cambridge University Press.

Bovensmann, H., Buchwitz, M., Burrows, J. P., Reuter, M., Krings, T. & Gerilowski, K. et al. (2010). A remote sensing technique for global monitoring of power plant CO2 emissions from space and related applications. *Atmospheric Measurement Techniques*, 3(4), 781-811. doi: 10.5194/amt-3-781-2010

Bovensmann, H., Burrows, J., Buchwitz, M., Frerick, J., Noël, S., & Rozanov, V. et al. (1999). SCIAMACHY: Mission Objectives and Measurement Modes. *Journal of The Atmospheric Sciences*, 56(2), 127-150. doi: 10.1175/1520-0469(1999)056<0127:smoamm>2.0.co;2

Buchwitz, M., Schneising, O., Burrows, J. P., Bovensmann, H., Reuter, M. & Notholt, J. (2007). First direct observation of the atmospheric CO_2 year-to-year increase from space. *Atmospheric Chemistry and Physics*, 7(16), 4249-4256. doi: 10.5194/acp-7-4249-2007

Buermann, W., Lintner, B., Koven, C., Angert, A., Pinzon, J., Tucker, C., & Fung, I. (2007). The changing carbon cycle at Mauna Loa Observatory. *Proceedings of The National Academy of Sciences*, 104(11), 4249-4254. doi: 10.1073/pnas.0611224104

Buschmann, M., Deutscher, N. M., Sherlock, V., Palm, M., Warneke, T. & Notholt, J. (2016). Retrieval of xCO_2 from ground-based mid-infrared (NDACC) solar absorption spectra and comparison to TCCON. *Atmospheric Measurement Techniques*, 9(2), 577-585. doi: 10.5194/amt-9-577-2016

Chhabra, A. & Gohel, A. (2017). Recent observations of atmospheric carbon dioxide over India, *Current Science*, 112(12), 2364–66.

Crisp, D., Atlas, R., Breon, F., Brown, L., Burrows, J. & Ciais, P. et al. (2004). The Orbiting Carbon Observatory (OCO) mission. *Advances in Space Research*, 34(4), 700-709. doi: 10.1016/j.asr.2003.08.062

Crisp, D., Pollock, H. R., Rosenberg, R., Chapsky, L., Lee, R. A. M. & Oyafuso, F. A. et al. (2017). The on-orbit performance of the Orbiting Carbon Observatory-2 (OCO-2) instrument and its radiometrically calibrated products. *Atmospheric Measurement Techniques*, 10(1), 59-81. doi: 10.5194/amt-10-59-2017

David, G., Miffre, A., Thomas, B., & Rairoux, P. (2012). Sensitive and accurate dual-wavelength UV-VIS polarization detector for optical remote sensing of tropospheric aerosols. *Applied Physics B*, *108*(1), 197-216. doi: 10.1007/s00340-012-5066-x

Dennison, P. E., Thorpe, A. K., Pardyjak, E. R., Roberts, D. A., Qi, Y. & Green, R. O. et al. (2013). High spatial resolution mapping of elevated atmospheric carbon dioxide using airborne imaging spectroscopy: Radiative transfer modeling and power plant plume detection. *Remote Sensing of Environment*, 139116-129. doi: 10.1016/j.rse.2013.08.001

Dettinger, M., & Ghil, M. (1998). Seasonal and interannual variations of atmospheric CO_2 and climate. *Tellus B*, 50(1), 1-24. doi: 10.1034/j.1600-0889.1998.00001.x

Deuzé, J., Bréon, F., Devaux, C., Goloub, P., Herman, M., Lafrance, B., Maignan, F., Marchand, A., Nadal, F., Perry, G. and Tanré, D., 2001. Remote sensing of aerosols over land surfaces from POLDER-ADEOS-1 polarized measurements. *Journal of Geophysical Research: Atmospheres*, 106(D5), pp.4913-4926.

Dubuisson, P., Frouin, R., Dessailly, D., Duforêt, L., Léon, J., Voss, K., & Antoine, D. (2009). Estimating the altitude of aerosol plumes over the ocean from reflectance ratio measurements in the O2 A-band. *Remote Sensing Of Environment*, *113*(9), 1899-1911. doi: 10.1016/j.rse.2009.04.018

Elachi, C., & Van Zyl, J. (2006). *Introduction to the physics and techniques of remote sensing* (2nd ed.). New Jersey & Canada: John Wiley & Sons, Inc.

Elias, T., & Roujean, J. (2008). Estimation of the aerosol radiative forcing at ground level, over land, and in cloudless atmosphere, from METEOSAT-7 observation: method and case study. *Atmospheric Chemistry And Physics*, *8*(3), 625-636. doi: 10.5194/acp-8-625-2008

EnviStats-India 2019, Vol. I: Environment Statistics. (2019). Retrieved from https://www.mospi.gov.in

Fu, Z., Dong, J., Zhou, Y., Stoy, P. C. & Niu, S. (2017). Long term trend and interannual variability of land carbon uptake—the attribution and processes. *Environmental Research Letters*, 12(1), 014018. doi: 10.1088/1748-9326/aa5685

Garg, A., Shukla, P., Kankal, B., & Mahapatra, D. (2017). CO_2 emission in India: trends and management at sectoral, sub-regional and plant levels. *Carbon Management*, 8(2), 111-123. doi: 10.1080/17583004.2017.1306406

Goetz, A. (2009). Three decades of hyperspectral remote sensing of the Earth: A personal view. *Remote Sensing of Environment*, 113, S5-S16. doi: 10.1016/j.rse.2007.12.014

Goetz, A., Vane, G., Solomon, J., & Rock, B. (1985). Imaging Spectrometry for Earth Remote Sensing. *Science*, 228(4704), 1147-1153. doi: 10.1126/science.228.4704.1147

Green, R. (2001). *Measuring the spectral expression of carbon dioxide in the solar reflected spectrum with AVIRIS*. Presentation, Proceedings of the 11th annual

Airborne Earth Science Workshop, Jet Propulsion Laboratory, California Institute of Technology, Pasadena, California 91109.

Green, R. O., Eastwood, M. L., Sarture, C. M., Chrien, T. G., Aronsson, M. & Chippendale, B. J. et al. (1998). Imaging Spectroscopy and the Airborne Visible/Infrared Imaging Spectrometer (AVIRIS). *Remote Sensing of Environment*, 65(3), 227-248. doi: 10.1016/s0034-4257(98)00064-9

Gupta, A., Dhaka, S. K., Matsumi, Y., Imasu, R., Hayashida, S. & Singh, V. (2019). Seasonal and annual variation of AIRS retrieved CO_2 over India during 2003–2011. *Journal of Earth System Science*, 128(4), doi: 10.1007/s12040-019-1108-7

Hakkarainen, J., Ialongo, I. & Tamminen, J. (2016). Direct space-based observations of anthropogenic CO_2 emission areas from OCO-2. *Geophysical Research Letters*, 43(21), doi: 10.1002/2016gl070885

Hakkarainen, J., Ialongo, I., Maksyutov, S., & Crisp, D. (2019). Analysis of Four Years of Global XCO_2 Anomalies as Seen by Orbiting Carbon Observatory-2. *Remote Sensing*, 11(7), 850. doi: 10.3390/rs11070850

Hamazaki, T., Kaneko, Y., & Kuze, A. (2004). *Carbon dioxide monitoring from the GOSAT satellite*. Presentation, Proceedings of XXth ISPRS Conference, Istanbul, Turkey.

Herzberg, G. (1944). *Atomic Spectra and Atomic Structure*. New York: Dover Publications.

Holben, B., Eck, T., Slutsker, I., Tanré, D., Buis, J., & Setzer, A. et al. (1998). AERONET—A Federated Instrument Network and Data Archive for Aerosol

Characterization. *Remote Sensing Of Environment*, *66*(1), 1-16. doi: 10.1016/s0034-4257(98)00031-5

Huang, X., Wang, T., Talbot, R., Xie, M., Mao, H. & Li, S. et al. (2015). Temporal characteristics of atmospheric CO_2 in urban Nanjing, China. *Atmospheric Research*, 153437-450. doi: 10.1016/j.atmosres.2014.09.007

Imasu, R. & Tanabe, Y. (2018). Diurnal and Seasonal Variations of Carbon Dioxide (CO_2) Concentration in Urban, Suburban, and Rural Areas around Tokyo. *Atmosphere*, 9(10), 367. doi: 10.3390/atmos9100367

Janardanan, R., Maksyutov, S., Oda, T., Saito, M., Kaiser, J., & Ganshin, A. et al. (2016). Comparing GOSAT observations of localized CO_2 enhancements by large emitters with inventory-based estimates. *Geophysical Research Letters*, 43(7), 3486-3493. doi: 10.1002/2016gl067843

Jensen, J. (2007). *Remote Sensing of the Environment: An Earth Resource Perspective* (2nd ed.). New Delhi, India: Pearson Education Singapore Pte. Ltd.

Jha, C., Thumaty, K., Rodda, S., Sonakia, A., & Dadhwal, V. (2013). Analysis of carbon dioxide, water vapour and energy fluxes over an Indian teak mixed deciduous forest for winter and summer months using eddy covariance technique. *Journal Of Earth System Science*, 122(5), 1259-1268. doi: 10.1007/s12040-013-0350-7

Jiang, X., Crisp, D., Olsen, E. T., Kulawik, S. S., Miller, C. E. & Pagano, T. S. et al. (2016). CO_2 annual and semiannual cycles from multiple satellite retrievals and models. *Earth and Space Science*, 3(2), 78-87. doi: 10.1002/2014ea000045

Jiang, X., Wang, J., Olsen, E. T., Liang, M., Pagano, T. S. & Chen, L. L. et al. (2013). Influence of El Niño on Midtropospheric CO_2 from Atmospheric Infrared Sounder

and Model. *Journal of the Atmospheric Sciences*, 70(1), 223-230. doi: 10.1175/jas-d-11-0282.1

Kaufman, Y., Tanré, D., Gordon, H., Nakajima, T., Lenoble, J., & Frouin, R. et al. (1997). Passive remote sensing of tropospheric aerosol and atmospheric correction for the aerosol effect. *Journal Of Geophysical Research: Atmospheres*, *102*(D14), 16815-16830. doi: 10.1029/97jd01496

Keeling, C., Bacastow, R., Bainbridge, A., Ekdahl, C., Guenther, P., Waterman, L., & Chin, J. (1976). Atmospheric carbon dioxide variations at Mauna Loa Observatory, Hawaii. *Tellus*, 28(6), 538-551. doi: 10.1111/j.2153-3490.1976.tb00701.x

Keeling, C., Chin, J., & Whorf, T. (1996). Increased activity of northern vegetation inferred from atmospheric CO_2 measurements. *Nature*, 382(6587), 146-149. doi: 10.1038/382146a0

Keeling, C., Piper, S., Bacastow, R., Wahlen, M., Whorf, T., Heimann, M., & Meijer, H. (2005). Atmospheric CO_2 and $^{13}CO_2$ Exchange with the Terrestrial Biosphere and Oceans from 1978 to 2000: Observations and Carbon Cycle Implications. *A History of Atmospheric CO_2 And Its Effects on Plants, Animals, and Ecosystems*, 83-113. doi: 10.1007/0-387-27048-5_5

Kleppner, D. (1999). A short history of atomic physics in the twentieth century. *Reviews Of Modern Physics*, 71(2), S78-S84. doi: 10.1103/revmodphys.71.s78

Kondratyev, K. Y. & Varotsos, C. (1995). Atmospheric greenhouse effect in the context of global climate change. *Il Nuovo Cimento C*, 18(2), 123-151. doi: 10.1007/bf02512015

Krapivin, V. F. & Varotsos, C. A. (2016). Modelling the CO_2 atmosphere-ocean flux in the upwelling zones using radiative transfer tools. *Journal of Atmospheric and Solar-Terrestrial Physics*, 150-15147-54. doi: 10.1016/j.jastp.2016.10.015

Kuze, A., Suto, H., Nakajima, M. & Hamazaki, T. (2009). Thermal and near infrared sensor for carbon observation Fourier-transform spectrometer on the Greenhouse Gases Observing Satellite for greenhouse gases monitoring. *Applied Optics*, 48(35), 6716. doi: 10.1364/ao.48.006716

Lee, E., Zeng, F., Koster, R. D., Weir, B., Ott, L. E. & Poulter, B. (2018). The impact of spatiotemporal variability in atmospheric CO_2 concentration on global terrestrial carbon fluxes. *Biogeosciences*, 15(18), 5635-5652. doi: 10.5194/bg-15-5635-2018

Li, K., Tian, B., Waliser, D. E. & Yung, Y. L. (2010). Tropical mid-tropospheric CO_2 variability driven by the Madden-Julian oscillation. *Proceedings of the National Academy of Sciences*, 107(45), 19171-19175. doi: 10.1073/pnas.1008222107

Li, Z., Xia, J., Ahlström, A., Rinke, A., Koven, C. & Hayes, D. J. et al. (2018). Non-uniform seasonal warming regulates vegetation greening and atmospheric CO_2 amplification over northern lands. *Environmental Research Letters*, 13(12), 124008. doi: 10.1088/1748-9326/aae9ad

Machida, T., Matsueda, H., Sawa, Y., Nakagawa, Y., Hirotani, K. & Kondo, N. et al. (2008). Worldwide Measurements of Atmospheric CO_2 and Other Trace Gas Species Using Commercial Airlines. *Journal of Atmospheric and Oceanic Technology*, 25(10), 1744-1754. doi: 10.1175/2008jtecha1082.1

Majumdar, D., & Gajghate, D. (2011). Sectoral CO_2, CH_4, N_2O and SO_2 emissions from fossil fuel consumption in Nagpur City of Central India. *Atmospheric Environment*, 45(25), 4170-4179. doi: 10.1016/j.atmosenv.2011.05.019

Marescaux, A., Thieu, V., Borges, A. V. & Garnier, J. (2018). Seasonal and spatial variability of the partial pressure of carbon dioxide in the human-impacted Seine River in France. *Scientific Reports*, 8(1), doi: 10.1038/s41598-018-32332-2

Matthais, V., Freudenthaler, V., Amodeo, A., Balin, I., Balis, D., & Bösenberg, J. et al. (2004). Aerosol lidar intercomparison in the framework of the EARLINET project 1 Instruments. *Applied Optics*, *43*(4), 961-976. doi: 10.1364/ao.43.000961

Monfray, P., Gaudry, A., Polian, G., & Lambert, G. (1987). Seasonal variations of atmospheric CO_2 in the southern Indian Ocean. *Tellus B: Chemical and Physical Meteorology*, 39(1-2), 67-71. doi: 10.3402/tellusb.v39i1-2.15323

Nevison, C. D., Mahowald, N. M., Doney, S. C., Lima, I. D., van, der Werf G. R. & Randerson, J. T. et al. (2008). Contribution of ocean, fossil fuel, land biosphere, and biomass burning carbon fluxes to seasonal and interannual variability in atmospheric CO_2. *Journal of Geophysical Research: Biogeosciences*, 113(G1), n/a-n/a. doi: 10.1029/2007jg000408

Patil, M., Dharmaraj, T., Waghmare, R., Prabha, T., & Kulkarni, J. (2014). Measurements of carbon dioxide and heat fluxes during monsoon-2011 season over rural site of India by eddy covariance technique. *Journal Of Earth System Science*, 123(1), 177-185. doi: 10.1007/s12040-013-0374-z

Piao, S., Liu, Z., Wang, Y., Ciais, P., Yao, Y. & Peng, S. et al. (2017). On the causes of trends in the seasonal amplitude of atmospheric CO_2. *Global Change Biology*, 24(2), 608-616. doi: 10.1111/gcb.13909

Publications Division, Ministry of Information and Broadcasting, Government of India. (2020). *India 2020*. New Delhi.

Ravi Kumar, K., Revadekar, J., & Tiwari, Y. (2014). AIRS retrieved CO_2 and its association with climatic parameters over India during 2004–2011. *Science of the Total Environment*, 476-477, 79-89. doi: 10.1016/j.scitotenv.2013.12.118

Ravi Kumar, K., Tiwari, Y., Revadekar, J., Vellore, R., & Guha, T. (2016). Impact of ENSO on variability of AIRS retrieved CO_2 over India. *Atmospheric Environment*, 142, 83-92. doi: 10.1016/j.atmosenv.2016.07.001

Raychaudhuri, B. & Roy, S. (2022). A Proof of Concept for Estimating the Annual Atmospheric Carbon Dioxide Variation from Orbiting Carbon Observatory-3 vEarly Data. *IEEE Geoscience and Remote Sensing Letters*, 191-5. doi: 10.1109/lgrs.2021.3099172

Raychaudhuri, B. (2016). Imaging spectroscopy: Origin and future trends. *Applied Spectroscopy Reviews, 51*(1), 23-35. doi: 10.1080/05704928.2015.1087405

Rees, W. (2001). *Physical Principles of Remote Sensing* (2nd ed.). U.K.: Cambridge University Press.

Remer, L., Kaufman, Y., Tanré, D., Mattoo, S., Chu, D., & Martins, J. et al. (2005). The MODIS Aerosol Algorithm, Products, and Validation. *Journal Of The Atmospheric Sciences*, *62*(4), 947-973. doi: 10.1175/jas3385.1

Revadekar, J., Ravi Kumar, K., Tiwari, Y., & Valsala, V. (2016). Variability in AIRS CO_2 during active and break phases of Indian summer monsoon. *Science of The Total Environment*, 541, 1200-1207. doi: 10.1016/j.scitotenv.2015.09.078

Román-Cascón, C., Yagüe, C., Arrillaga, J., Lothon, M., Pardyjak, E. & Lohou, F. et al. (2019). Comparing mountain breezes and their impacts on CO_2 mixing ratios at three contrasting areas. *Atmospheric Research*, 221111-126. doi: 10.1016/j.atmosres.2019.01.019

Roy, P., Behera, M., Murthy, M., Roy, A., Singh, S. & Kushwaha, S. et al. (2015). New vegetation type map of India prepared using satellite remote sensing: Comparison with global vegetation maps and utilities. *International Journal of Applied Earth Observation and Geoinformation*, 39, 142-159. doi: 10.1016/j.jag.2015.03.003

Sanghavi, S., Martonchik, J., Landgraf, J., & Platt, U. (2012). Retrieval of the optical depth and vertical distribution of particulate scatterers in the atmosphere using O_2 A- and B-band SCIAMACHY observations over Kanpur: a case study. *Atmospheric Measurement Techniques*, *5*(5), 1099-1119. doi: 10.5194/amt-5-1099-2012

Schawlow, A. (1982). Spectroscopy in a new light. *Reviews Of Modern Physics*, 54(3), 697-707. doi: 10.1103/revmodphys.54.697

Schott, J. (2007). *Remote Sensing: The Image Chain Approach* (2nd ed.). New York: Oxford University Press.

Singh, R., Janmaijaya, M., Dhaka, S., & Kumar, V. (2015). Study on the association of greenhouse gas (CO_2) with monsoon rainfall using AIRS and TRMM satellite observations. *Physics And Chemistry of The Earth, Parts A/B/C*, 89-90, 65-72. doi: 10.1016/j.pce.2015.04.004

Thorpe, A. K., Frankenberg, C., Thompson, D. R., Duren, R. M., Aubrey, A. D. & Bue, B. D. et al. (2017). Airborne DOAS retrievals of methane, carbon dioxide, and water vapor concentrations at high spatial resolution: application to AVIRIS-NG. *Atmospheric Measurement Techniques*, 10(10), 3833-3850. doi: 10.5194/amt-10-3833-2017

Tiwari, Y. K., Revadekar, J. & Ravi, Kumar K. (2013). Variations in atmospheric Carbon Dioxide and its association with rainfall and vegetation over India. *Atmospheric Environment*, 6845-51. doi: 10.1016/j.atmosenv.2012.11.040

Tiwari, Y., Vellore, R., Ravi Kumar, K., van der Schoot, M., & Cho, C. (2014). Influence of monsoons on atmospheric CO_2 spatial variability and ground-based monitoring over India. *Science of The Total Environment*, 490, 570-578. doi: 10.1016/j.scitotenv.2014.05.045

Umezawa, T., Matsueda, H., Sawa, Y., Niwa, Y., Machida, T., & Zhou, L. (2018). Seasonal evaluation of tropospheric CO_2 over the Asia-Pacific region observed by the CONTRAIL commercial airliner measurements. *Atmospheric Chemistry and Physics*, 18(20), 14851-14866. doi: 10.5194/acp-18-14851-2018

Vane, G., & Goetz, A. (1993). Terrestrial imaging spectrometry: Current status, future trends. *Remote Sensing of Environment*, 44(2-3), 117-126. doi: 10.1016/0034-4257(93)90011-l

Vane, G., Goetz, A., & Wellman, J. (1984). Airborne imaging spectrometer: A new tool for remote sensing. *IEEE Transactions on Geoscience and Remote Sensing*, GE-22(6), 546-549. doi: 10.1109/tgrs.1984.6499168

Varotsos, C., Assimakopoulos, M. & Efstathiou, M. (2006). Technical Note: Long-term memory effect in the atmospheric CO_2 concentration at Mauna Loa. doi: 10.5194/acpd-6-11957-2006

Watanabe, H., Hayashi, K., Saeki, T., Maksyutov, S., Nasuno, I. & Shimono, Y. et al. (2015). Global mapping of greenhouse gases retrieved from GOSAT Level 2 products by using a kriging method. *International Journal of Remote Sensing*, 36(6), 1509-1528. doi: 10.1080/01431161.2015.1011792

Wei, J., Savtchenko, A., Vollmer, B., Hearty, T., Albayrak, A. & Crisp, D. et al. (2014). Advances in CO_2 observations from AIRS and ACOS. *IEEE Geoscience and Remote Sensing Letters*, 11(5), 891-895. doi: 10.1109/lgrs.2013.2281147

Wunch, D., Toon, G. C., Blavier, J. L., Washenfelder, R. A., Notholt, J. & Connor, B. J. et al. (2011). The Total Carbon Column Observing Network. *Philosophical Transactions of the Royal Society A: Mathematical, Physical and Engineering Sciences*, 369(1943), 2087-2112. doi: 10.1098/rsta.2010.0240

Wunch, D., Wennberg, P., Osterman, G., Fisher, B., Naylor, B., & Roehl, C. et al. (2016). Comparisons of the Orbiting Carbon Observatory-2 (OCO-2) X_{CO2} measurements with TCCON. *Atmospheric Measurement Techniques*, 10, 2209–2238. doi: 10.5194/amt-2016-227

Xueref-Remy, I., Dieudonné, E., Vuillemin, C., Lopez, M., Lac, C. & Schmidt, M. et al. (2018). Diurnal, synoptic and seasonal variability of atmospheric CO_2 in the Paris megacity area. *Atmospheric Chemistry and Physics*, 18(5), 3335-3362. doi: 10.5194/acp-18-3335-2018

Yokota, T., Yoshida, Y., Eguchi, N., Ota, Y., Tanaka, T. & Watanabe, H. et al. (2009). Global Concentrations of CO_2 and CH_4 Retrieved from GOSAT: First Preliminary Results. *SOLA*, 5160-163. doi: 10.2151/sola.2009-041

Yoshida, Y., Ota, Y., Eguchi, N., Kikuchi, N., Nobuta, K. & Tran, H. et al. (2011). Retrieval algorithm for CO_2 and CH_4 column abundances from short-wavelength infrared spectral observations by the Greenhouse gases observing satellite. *Atmospheric Measurement Techniques*, 4(4), 717-734. doi: 10.5194/amt-4-717-2011

Zhang, X., Gurney, K. R., Rayner, P., Baker, D. & Liu, Y. (2016). Sensitivity of simulated CO_2 concentration to sub-annual variations in fossil fuel CO_2 emissions. *Atmospheric Chemistry and Physics*, 16(4), 1907-1918. doi: 10.5194/acp-16-1907-2016

Zhao, F. & Zeng, N. (2014). Continued increase in atmospheric CO_2 seasonal amplitude in the 21st century projected by the CMIP5 Earth system models. *Earth System Dynamics*, 5(2), 423-439. doi: 10.5194/esd-5-423-2014